THE JOURNAL OF PHYSICAL CHEMISTRY C

ARTICLE

pubs.acs.org/JPCC

Direct Evidence for the Instability and Deactivation of Mixed-Oxide Systems: Influence of Surface Segregation and Subsurface Diffusion

Emre Emmez,[†] Evgeny I. Vovk,[†,‡] Valerii I. Bukhtiyarov,[‡] and Emrah Ozensoy*[,†]

[†]Chemistry Department, Bilkent University, 06800 Bilkent, Ankara, Turkey

[‡]Boreskov Institute of Catalysis, 630090 Novosibirsk, Russian Federation

ABSTRACT:

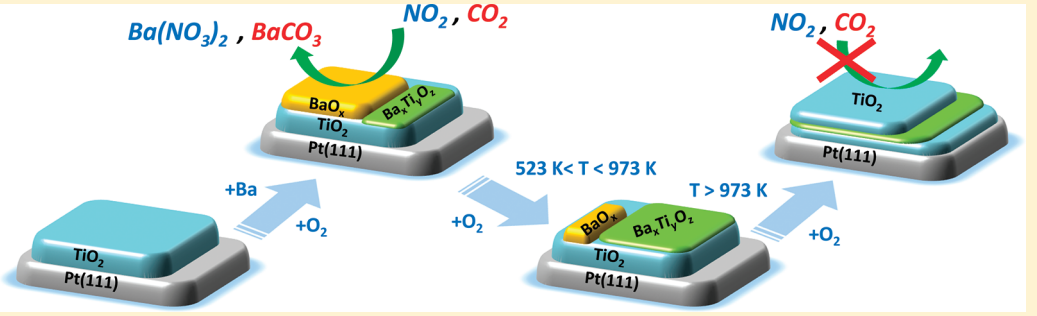

In the current contribution, we provide a direct demonstration of the thermally induced surface structural transformations of an alkaline-earth oxide/transition metal oxide interface that is detrimental to the essential catalytic functionality of such mixed-oxide systems toward particular reactants. The $BaO_x/TiO_2/Pt(111)$ surface was chosen as a model interfacial system where the enrichment of the surface elemental composition with Ti atoms and the facile diffusion of Ba atoms into the underlying TiO_2 matrix within 523−873 K leads to the formation of perovskite type surface species ($BaTiO_3/Ba_2TiO_4/Ba_xTi_yO_z$). At elevated temperatures (T > 973 K), excessive surface segregation of Ti atoms results in an exclusively TiO_2/TiO_x-terminated surface which is almost free of Ba species. Although the freshly prepared $BaO_x/TiO_2/Pt(111)$ surface can strongly adsorb ubiquitous catalytic adsorbates such as NO_2 and CO_2, a thermally deactivated surface at T > 973 K practically loses all of its NO_2/CO_2 adsorption capacity due to the deficiency of surface BaO_x domains.

1. INTRODUCTION

A molecular-level understanding of the fundamental interactions between different metal-oxide domains coexisting on surfaces is crucial in order to improve the performance of functional materials and to design new systems with unprecedented capabilities that can be used in electronics, sensor applications, high temperature superconductivity, energy conversion, fuel cells, photovoltaics, and heterogeneous catalysis.[1−5] Alkaline-earth oxide/transition metal oxide interfaces play a central role in most of these applications where understanding and controlling the surface structure and the surface transformations seems to be the ultimate challenge for improving the state of the art in such systems. Along these lines, in the current work, we have focused our attention on a representative model alkaline-earth oxide/transition metal oxide interface (i.e., $BaO_x/TiO_2/Pt(111)$) and investigated fundamental thermally induced surface structural changes by presenting a direct demonstration of the thermal catalytic deactivation of these mixed-oxide systems due to subsurface diffusion and surface segregation phenomena. Although the implications of the demonstrated surface transformations are currently discussed in the context of heterogeneous catalysis, significant ramifications of the observed results can be certainly envisaged in a large number of applications exploiting analogous families of mixed-oxide interfaces.

2. EXPERIMENTAL SECTION

All experiments were performed in a custom-made ultra high vacuum (UHV) chamber with a base pressure of 2×10^{-10} Torr. The UHV chamber is equipped with X-ray photoelectron spectroscopy (XPS), rear-view low energy electron diffraction (LEED), and temperature programmed desorption (TPD) techniques. XPS spectra were recorded using a Riber cylindrical mirror analyzer and a nonmonochromated X-ray source using Al Kα X-ray irradiation ($h\nu$ = 1486.6 eV, 300 W). A Dycor DM200 M quadrupole mass spectrometer (QMS) was used for the TPD experiments. A Pt(111) single crystal (10 mm diameter, 2 mm thickness, both sides atomically polished, MaTeck GmbH) was used as the substrate in the current studies. The Pt(111) single crystal was mounted on a tantalum wire assembled to a high-precision manipulator. The heating of the sample was achieved by direct resistive heating of the sample. The sample temperature was monitored by a K-Type thermocouple spot-welded onto the lateral edge of the crystal. The Pt(111) surface was cleaned by multiple cycles of Ar^+ sputtering at 1.5 kV and subsequent

Received: July 21, 2011
Revised: September 30, 2011
Published: October 10, 2011

dx.doi.org/10.1021/jp206969h | J. Phys. Chem. C 2011, 115, 22438–22443

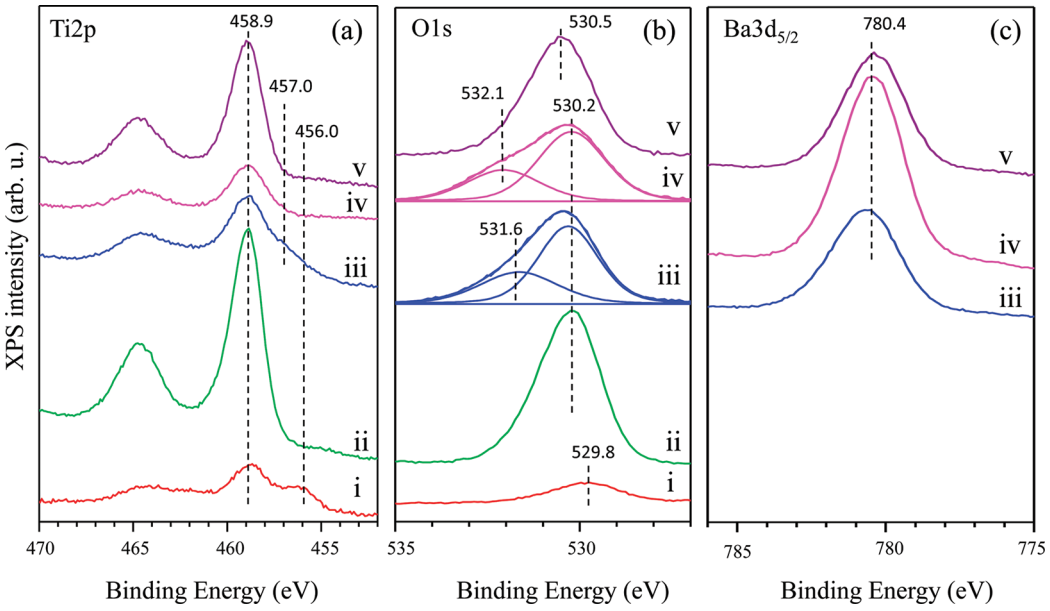

Figure 1. XPS data corresponding to the (a) Ti2p, (b) O1s, and (c) $Ba3d_{5/2}$ regions obtained for (i) TiO_x(1.4 MLE)/Pt(111), (ii) TiO_2(26 MLE)/Pt(111), (iii) as deposited Ba(3 MLE)/ TiO_2(26 MLE)/ Pt(111) surface prior to oxidation, (iv) BaO_x(6 MLE)/TiO_2(26 MLE)/Pt(111) surface obtained after oxidizing the sample (iii) in O_2 ($P_{O_2} = 5 \times 10^{-7}$ Torr) at 523 K followed by a second Ba deposition at RT and oxidation at 523 K, and (v) a surface prepared by the oxidation of sample (iv) in O_2 ($P_{O_2} = 5 \times 10^{-7}$ Torr) at 973 K.

heating to 1073 K in vacuum. The cleanness of the surface was confirmed by XPS and LEED.

TiO_2 films on Pt(111) were grown by thermal evaporation using a Ti wire (99.6% purity, Mateck GmbH) on a clean Pt(111) surface at room temperature in vacuum and subsequent oxidation in 5×10^{-7} Torr of O_2 (99.999% purity, Linde AG) at 973 K. TiO_2 film thickness was estimated via the attenuation of the $Pt4f_{7/2}$ XPS signal using the equation[6]

$$d_{ox} = \lambda \sin\theta \ln[((I_{Pt}^{\infty} - I_{Pt})/I_{Pt}) + 1] \quad (1)$$

where λ is the inelastic mean free path of the $Pt4f_{7/2}$ photoelectrons in the oxide film determined via QUASES-IMFP-TPP2M Ver 2.2 software[7] (2.7 nm), θ is the take off angle between the surface plane and the outgoing photoelectrons (i.e., 48°), I_{Pt}^{∞} is the intensity of the $Pt4f_{7/2}$ signal for a clean Pt(111) surface, and I_{Pt} is the intensity of the $Pt4f_{7/2}$ signal for the TiO_2/Pt(111) surface.

BaO_x layers on TiO_2/Pt(111) were prepared by thermal evaporation of Ba from a $BaAl_4$ alloy (ST2/FR wire, SAES Getters) at room temperature and subsequent oxidation in 5×10^{-7} Torr O_2 at 523 K. BaO coverages on the TiO_2/Pt(111) were estimated using two independent ways in order to cross-check the calculated coverage values. In the first method, BaO film thickness on TiO_2/ Pt(111) was calculated via eq 1, where the attenuation of the $Ti2p_{3/2}$ signal was used instead of $Pt4f_{7/2}$. In the second method, BaO thickness was estimated by calibrating the dosing rate of the Ba doser on the clean Pt(111) surface and then calculating the Ba approximate coverage on the TiO_2/Pt(111) surface based on the Ba dosing duration and the Ba doser heating current (c.a. 10.0 A). BaO film thickness values obtained by these two independent methods were in good agreement with each other (i.e., with a difference of less than 25%).

In order to estimate the coverage of TiO_2 overlayers in terms of monolayer equivalents (MLE) from the calculated film thickness (d_{ox} in eq 1), the ML thickness of TiO_2 was taken to be 0.325 nm, corresponding to interlayer spacing in the ⟨110⟩ direction in the bulk rutile TiO_2 crystal. For BaO coverage calculations, the ML thicknesses were taken to be 0.39 nm, corresponding to the interlayer spacing in the ⟨110⟩ direction in the bulk BaO crystal. The rutile (110) surface parameters were used in the calculations since this surface is probably one of the most thoroughly investigated titania surfaces in the literature with well-defined parameters, whereas the BaO(110) surface parameters were used since this surface was observed to form on the Pt(111) surface in our recent studies.[8] For reference, 1 ML of TiO_2 rutile (110) surface corresponds to 1.04×10^{15} Ti atoms/cm^2, 1 ML of BaO (110) surface corresponds to 0.47×10^{15} Ba atoms/cm^2, and 1 ML of Pt(111) corresponds to 1.5×10^{15} atoms/cm^2.

NO_2 gas, used in the experiments, was synthesized by the reaction of NO (99.9% purity, Air Products) with O_2 and further purification by subsequent freeze−thaw−pump cycles. CO_2 gas (Linde AG, Purity 99,999%) was used without further purification.

3. RESULTS AND DISCUSSION

Figure 1 presents the XPS data obtained during the growth of the TiO_2/Pt(111) and BaO_x/TiO_2/Pt(111) surfaces. Figure 1a (spectrum i) demonstrates that during the initial stages of the TiO_x film growth Ti sites are partially oxidized, which is evident from the existence of both Ti^{4+} (458.9 eV) and Ti^{3+} (456.0 eV) $Ti2p_{3/2}$ signals, whereas a fully oxidized thick (c.a. 26 MLE) TiO_2 film (Figure 1a, spectrum ii) reveals exclusively Ti^{4+} signal. Evaporation of metallic Ba (3 MLE) on the TiO_2/Pt(111) surface at room temperature (RT) clearly induces a partial reduction of the titania film and the formation of reduced $Ti2p_{3/2}$ states within the range of 457.0−456.0 eV (Figure 1a, spectrum iii). After the oxidation of the Ba overlayer in O_2 ($P_{O_2} = 5 \times 10^{-7}$ Torr) at 523 K followed by a second Ba deposition and oxidation step at 523 K (resulting in a Ba coverage of ca. 6 MLE) (Figure 1a, spectrum iv), almost all of the Ti sites are oxidized to Ti^{4+}, whereas the intensities of all of the Ti2p signal visibly

dx.doi.org/10.1021/jp206969h |J. Phys. Chem. C 2011, 115, 22438–22443

decreases. On the other hand, a further oxidation step (Figure 1a, spectrum v) at 973 K in O_2 ($P_{O_2} = 5 \times 10^{-7}$ Torr) drastically increases the intensities of the Ti2p signals revealing a spectrum with a close resemblance to that of a fully oxidized thick TiO_2 film on Pt(111) (Figure 1a, spectrum ii).

When the O1s region of the XP spectrum is investigated for the same series of experiments, it is seen that the thick TiO_2 film on Pt(111) (Figure 1b, spectrum ii) reveals an O1s signal at 530.2 eV, consistent with an almost fully oxidized TiO_2 film.[9] Ba dosing at RT (Figure 1b, spectrum iii) gives rise to the broadening of the O1s signal at 530.2 eV most likely due to the partial oxidation of Ba to form $BaO/BaO_2/BaO_x$ (the characteristic O1s signal for BaO appears at 528.5−529.5 eV, and the signal for BaO_2 appears at a 1.8−2.5 eV higher binding energy (BE)[10,11]). An additional shoulder which becomes visible at 531.6 eV in Figure 1b, spectrum iii, can be ascribed to perovskite-type surface species ($BaTiO_3/Ba_2TiO_4/Ba_xTi_yO_z$).[12] It is worth mentioning that Ba_2TiO_4 (barium orthotitanate) is a metastable phase that has been reported[13] to precede $BaTiO_3$ formation during the reaction between $BaO/BaCO_3$ and TiO_2 at elevated temperatures. Oxidation of this Ba overlayer with O_2 followed by an additional Ba evaporation and oxidation step at 523 K (Figure 1b, spectrum iv) accentuates and shifts the shoulder to 532.1 eV suggesting an increase in the surface population of perovskite-like surface domains. After oxidation at 973 K (Figure 1b, spectrum v), the Ti2p signal reveals a pronounced increase and the shoulder at 532.1 eV almost completely disappears, yielding an O1s spectrum that is quite similar to that of TiO_2/Pt(111) (Figure 1b, spectrum ii).

Ba $3d_{5/2}$ spectra given in Figure 1c are in good agreement with the observations discussed above. After the initial deposition of the Ba on TiO_2/Pt(111) at RT (Figure 1c, spectrum iii), the $Ba3d_{5/2}$ signal at 780.6 eV is detected. Although the BE of this feature does not significantly shift after oxidation−Ba deposition−oxidation procedure (Figure 1c, spectrum iv), its intensity increases in a pronounced manner which is attributed to the additional dose of Ba and an improved forward photoelectron scattering due to the increasing wetting/surface dispersion of the $BaO_x/Ba_xTi_yO_z$ domains. In contrast, oxidation at 973 K prompts a significant attenuation of the Ba $3d_{5/2}$ signal (Figure 1c, spectrum v).

In the light of the observations presented above, it can be argued that metallic Ba adsorption on the TiO_2/Pt(111) surface at RT in vacuum induces a strong interaction between surface O^{2-} sites and Ba atoms, oxidizing the Ba^0 species while reducing the Ti^{4+} sites. Oxidation of this surface with O_2 at an intermediate temperature such as 523 K triggers the formation of BaO_x as well as perovskite-type mixed oxide domains such as $BaTiO_3$, Ba_2TiO_4, and possibly their defective forms ($Ba_xTi_yO_z$). Decrease in the Ti2p signal after Ba deposition at RT and oxidation at 523 K in comparison to the clean TiO_2/Pt(111) surface is in agreement with the fact that the titania layer resides below the $BaO_x/Ba_xTi_yO_z$ overlayer under these conditions. Meanwhile, increasing the oxidation temperature to 973 K results in a drastic change in the surface composition. This is evident from the considerable decrease in the Ba $3d_{5/2}$ signal intensity, concomitant to a significant rise in the Ti2p signal intensity. These observations can be explained by the segregation of the Ti sites to the topmost surface and the diffusion of $BaO_x/Ba_xTi_yO_z$ domains beneath the TiO_2 overlayer, giving rise to a TiO_2-terminated surface.

The temperature-dependent structural changes on the BaO_x/TiO_2/Pt(111) surface were also further investigated via LEED (Figure 2). Figure 2a presents the LEED image corresponding to a thick (ca. 26 MLE) TiO_2 film grown on a clean Pt(111)

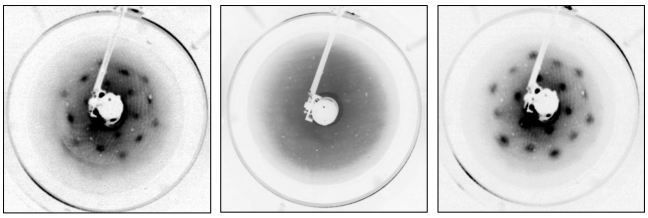

Figure 2. LEED images corresponding to (a) (2 × 2) TiO_2(26 MLE)/Pt(111), (b) BaO_x(<1 MLE)/TiO_2(26 MLE)/Pt(111), (c) a surface obtained by the oxidation of sample (b) in O_2 ($P_{O_2} = 5 \times 10^{-7}$ Torr) at 1073 K. LEED patterns were recorded using electron energy values of 85, 85, and 105 eV, respectively.

substrate as described above. In spite of the significant thickness of the TiO_2 overlayer, broad but clearly discernible LEED spots are apparent in Figure 2a, indicating the presence of a long-range ordering in the TiO_2 film revealing a (2 × 2) structure. A similar c(2 × 2) reconstruction has also been observed on a rutile TiO_2(100) surface.[14,15] Former reports in the literature demonstrated that TiO_2 ultrathin films grown on Pt(111) can exhibit a variety of ordered structures.[16,17] For instance, TiO_2 ultrathin films grown on Pt(111) with a titania overlayer coverage of 0.8 ML present a LEED diffraction revealing zigzag-like TiO_x features which is also referred as the "z-TiO_x" overlayer.[16] This so-called z-overlayer was assigned to an incommensurate superstructure with respect to the Pt(111) substrate with a rectangular unit cell of about (6.8 ± 0.1) × (8.6 ± 0.1) Å^2.[17] Former STM studies in the literature also suggested that the z-TiO_x structure was comprised of an O−Ti bilayer, with an oxygen termination.[16] Other ordered TiO_2 overlayers on Pt(111) were also observed in the literature[16] for a TiO_2 overlayer coverage of 1.2 MLE. This latter ordered overlayer was called wagon-wheel-like or w-TiO_x structure.[16] A detailed analysis of this w-TiO_x/Pt(111) surface revealed that w-TiO_x overlayer formed an ordered ($\sqrt{43} \times \sqrt{43}$) R 7.6° structure with a unit vector of 18.2 Å.[16]

The ordered overlayer in Figure 2a is lost when Ba (<1 MLE) is deposited on TiO_2/Pt(111) and oxidized at 523 K in O_2 (Figure 2b) suggesting that BaO_x-$Ba_xTi_yO_z$ overlayer on TiO_2/Pt(111) has an amorphous structure. Interestingly, oxidation of the BaO_x−$Ba_xTi_yO_z$ overlayer on TiO_2/Pt(111) at 1073 K in O_2 regenerates the (2 × 2) LEED pattern that is obtained for the clean TiO_2/Pt(111) surface. These LEED results are in agreement with the conclusion that oxidation of the $BaO_x/Ba_xTi_yO_z$ overlayers on TiO_2/Pt(111) gives rise to the diffusion of the $BaO_x/Ba_xTi_yO_z$ domains into the TiO_2 matrix leading to the segregation of Ti sites on the surface and the formation of a TiO_2-terminated overlayer. Reconstruction of perovskite surfaces and the formation of TiO_2/TiO-terminated surface structures at elevated temperatures have also been reported for $SrTiO_3$(001)[18,19] and $SrTiO_3$(111)[20] surfaces. TiO_2-terminated surfaces have been observed for the (2 × 1) reconstruction[18] and the c(4 × 2) reconstruction of $SrTiO_3$(001) at elevated temperatures,[19] and a TiO(111)-(2 × 2) terminated reconstructed surface was observed on $SrTiO_3$(111).[20]

We have investigated these thermally induced structural changes for a variety of temperatures in which we have monitored the Ba/Ti surface atomic ratio via XPS after oxidation steps carried out at temperatures ranging from 300 to 1073 K. In these experiments Ba with an estimated coverage of <1 MLE was

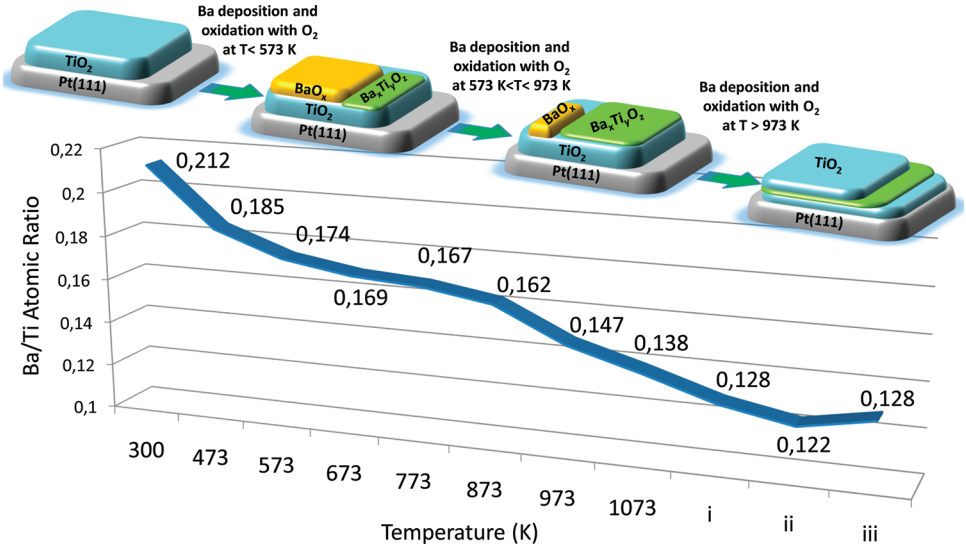

Figure 3. Ba/Ti surface atomic ratio values obtained from the XPS data for a BaO_x(<1 MLE)/TiO_2(26 MLE)/Pt(111) surface after various oxidation and thermal aging steps at various temperatures (see text for details).

deposited on a TiO_2(26 MLE)/Pt(111) surface. As summarized in Figure 3, Ba/Ti surface atomic ratio displays a monotonic decrease with increasing oxidation temperatures. Note that the oxidation steps were typically performed with an O_2 partial pressure of 5×10^{-7} Torr and for durations of 20 min. Sample i in Figure 3 was treated with O_2 at 1073 K for 30 min. Sample ii was obtained by annealing sample i in vacuum at 1073 K for 30 min, and sample iii was obtained by dosing 1×10^{-7} Torr NO_2 (a more aggressive oxidizing agent than O_2) on sample ii at a temperature of 300 K for 30 min followed by annealing at 1073 K (to further oxidize the surface and desorb the residual NO_x species). Figure 3 reveals that, even after the oxidation steps at relatively low temperatures ($T < 573$ K), a rather sharp decrease in the Ba/Ti surface atomic ratio is visible, indicating that the Ba diffusion into the TiO_2 matrix has a rather small activation barrier and is likely to occur even at relatively low temperatures. Note that the Ba/Ti surface atomic ratio variation under these conditions may partly be ascribed to the agglomeration of the BaO domains and sintering; however, observed changes in the O1s region in XPS definitely indicate the presence of additional surface phenomena such as the formation of perovskite-type species due to BaO diffusion and reaction with the TiO_2 matrix. Under these low-temperature oxidation conditions, the surface is dominated with BaO_x species with a smaller contribution from $Ba_xTi_yO_z$ domains. Figure 3 also reveals that the Ba/Ti surface atomic ratio is observed to stay fairly stable within a broad band of intermediate temperatures (i.e., 573−873 K). Within this temperature window, current XPS results indicate that the surface contains a larger contribution from perovskite-type species ($Ba_xTi_yO_z$). At oxidation temperatures above 873 K, a steep decline in the Ba/Ti surface atomic ratio is visible suggesting a fast and an efficient diffusion of Ba sites into the underlying TiO_2 framework. It is also apparent in Figure 3 that, after extended oxidation and/or annealing steps performed at 1073 K, Ba/Ti surface atomic ratio reaches a rather steady value where the surface is characterized by LEED pattern presented in Figure 2c and its XPS analysis reveals similar characteristics to the topmost XPS spectra in Figure 1.

Chemical reactivity of the $BaO_x/Ba_xTi_yO_z$ overlayers on TiO_2/Pt(111) were also studied toward various ubiquitous adsorbates in heterogeneous catalysis (i.e., NO_2 and CO_2) which are relevant to numerous catalytic systems including (but not limited to) NO_x-storage reduction systems.[21−26] In order to achieve this, adsorption experiments were performed by saturating the surfaces with either NO_2 or CO_2 at RT ($P_{NO_2} = 1 \times 10^{-7}$ Torr for 30 min at RT and $P_{CO_2} = 5 \times 10^{-7}$ Torr for 5 min at RT) and then monitoring the desorption profiles at elevated temperatures via TPD. Figure 4a depicts a TPD profile obtained after NO_2 saturation of a BaO_x(6 MLE)/TiO_2(26 MLE)/Pt(111) surface at RT. On the basis of the current XPS results, this surface is dominated by BaO_x domains with a smaller contribution from $Ba_xTi_yO_z$ domains. TPD spectrum given in Figure 4a, spectrum i, corresponding to $m/z = 30$, clearly indicates that this surface can efficiently store NO_2 most likely in the form of nitrates resulting in a desorption maximum at 635 K that is consistent with the strongly bound ionic NO_3^-/NO_2^- species adsorbed on BaO_x[25] and $Ba_xTi_yO_z$ domains.[28] It should be mentioned that, although NO_x storage capacity of supported BaO surfaces are typically higher than that of $BaTiO_3$, $BaTiO_3$ surfaces can also store appreciable amount of NO_2 or CO_2 in the form of nitrates/nitrites or carbonates, respectively. This might be partly ascribed to the BaO termination of the $BaTiO_3$(100) surface.[29] It is also worth mentioning that no oxygen ($m/z = 32$) evolution was detected in this TPD experiment suggesting that the oxygen atoms produced during the decomposition of nitrates/nitrites are either dissolved in the subsurface or take part in the oxidation of BaO to BaO_2 as commonly observed in the case of NO_2 desorption from BaO overlayers.[8,23,24] TPD profile given in Figure 4a, spectrum ii ($m/z = 30$) was obtained by saturating the surface given in spectrum i with NO_2 after the first TPD run (in other words, spectrum ii corresponds to the second successive NO_2−TPD of the freshly prepared surface). It is evident from Figure 4a, spectrum ii that the NO_x uptake capacity of the surface is almost completely lost after the first TPD run due to the formation of a TiO_2-terminated surface and the diffusion of surface Ba sites into the subsurface. In order to demonstrate the relatively small NO_2 adsorption capacity of TiO_2-terminated surfaces compared to that of BaO_x terminated surfaces, we have also performed a control experiment in which NO_2 was adsorbed on

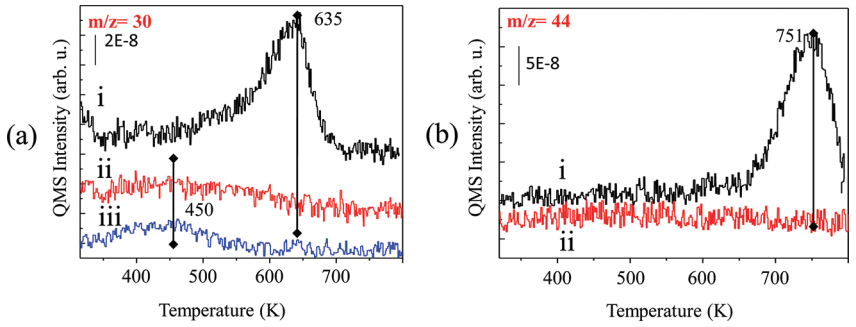

Figure 4. (a) $m/z = 30$ desorption channel in the TPD profiles for NO_2 adsorption ($P_{NO_2} = 1 \times 10^{-7}$ Torr for 30 min at RT) on fresh BaO_x(6 MLE)/TiO_2(26 MLE)/Pt(111) surface (spectrum i), BaO_x(6 MLE)/TiO_2(26 MLE)/Pt(111) surface pretreated at 973 K (spectrum ii), and fresh TiO_2(26 MLE)/Pt(111) surface (spectrum iii). (b) $m/z = 44$ desorption channels in the TPD profiles for CO_2 adsorption ($P_{CO_2} = 5 \times 10^{-7}$ Torr for 5 min at RT) on: fresh BaO_x(6 MLE)/TiO_2(26 MLE)/Pt(111) surface (spectrum i), BaO_x(6 MLE)/TiO_2(26 MLE)/Pt(111) surface pretreated at 973 K (spectrum ii).

a TiO_2(26 MLE)/Pt(111) surface at RT (Figure 4a, spectrum iii). In this control experiment, a characteristically weak $m/z = 30$ desorption signal was detected with a significantly lower desorption maximum within 400-450 K pointing to the fact that the saturation coverage and the adsorption strength of adsorbed NO_x species on a TiO_2-terminated TiO_2/Pt(111) surface at RT is much smaller compared to that of BaO_x/TiO_2/Pt(111) (Figure 4a, spectrum i) and BaO_x/Pt(111)[8] surfaces.

This observation is also in perfect agreement with the additional TPD experiments performed by saturating the surfaces given in Figure 4a, spectra i and ii with CO_2 at RT (Figure 4b). Figure 4b, spectrum i reveals a strong $m/z = 44$ desorption signal at 751 K, associated with the decomposition of strongly bound ionic carbonate-like surface species. It is also crucial to emphasize that the CO_2 uptake of the surface given in Figure 4b, spectrum i seems to be completely suppressed after annealing at 973 K (Figure 4b, spectrum ii). The reason for the suppression of CO_2 uptake is also associated with the formation of a Ti-enriched surface overlayer on a thermally aged BaO_x/TiO_2/Pt(111) system.

4. CONCLUSIONS

Current results shed light on the fundamental aspects of the thermally induced surface structural transformations of alkaline earth oxide/transition metal oxide interfaces and provide valuable insights regarding their catalytic deactivation pathways. By utilizing the BaO_x/TiO_2/Pt(111) model system, it was demonstrated that perovskite-type surface species (i.e., $BaTiO_3/Ba_2TiO_4/Ba_xTi_yO_z$) form even at temperatures as low as 523 K, concomitant to the diffusion of $BaO_x/Ba_xTi_yO_z$ species into the underlying TiO_2 framework. Diffusion of Ba-containing species into the TiO_2 framework is further facilitated at $T > 873$ K. These surface phenomena result in a TiO_2-terminated surface which is almost completely deficient of Ba-containing domains exposed on the surface. The surface segregation of TiO_2 species yields a surface structure that is incapable of performing some of the vital catalytic functions of the investigated alkaline earth oxide/transition metal oxide interface, such as NO_2/CO_2 adsorption and storage. Currently observed surface phenomena unveil a general behavior that has direct potential implications in high temperature superconductivity, solid oxide fuel cells (SOFC), sensors, and electronic device applications. Further surface scientific investigations are required in order to elucidate and control such surface/subsurface diffusion phenomena and diffusion kinetics and to design advanced structural promoters that can act as diffusion barriers[30,31] in mixed oxide interfacial systems.

AUTHOR INFORMATION

Corresponding Author

*E-mail: ozensoy@fen.bilkent.edu.tr.

ACKNOWLEDGMENT

Authors acknowledge the financial support from TUBITAK (Grant No. 107Y115) and RFBR (No. 09-03-91225-CT_a and No. 10-03-00596-a). E.O. also acknowledges support from Turkish Academy of Sciences for the "Outstanding Young Investigator" Grant. Authors also gratefully acknowledge Prof. Mehmet Erbudak (ETH, Zurich) for his help with the LEED and XPS measurements and for fruitful discussions.

REFERENCES

(1) Mathews, S.; Ramesh, R.; Venkatesan, T.; Benedetto, J. *Science* **1997**, *276*, 238.
(2) Takata, T.; Domen, K. *J. Phys. Chem. C* **2009**, *113*, 19386.
(3) Raj, E. S.; Pratt, K. F. E.; Skinner, S. J.; Parkin, I. P.; Kilner, J. A. *Chem. Mater.* **2006**, *18*, 3351.
(4) Larbalestier, D.; Gurevich, A.; Feldmann, D. M.; Polyanskii, A. *Nature* **2001**, *414*, 368.
(5) Mamak, M.; Metraux, G. S.; Petrov, S.; Coombs, N.; Ozin, G. A.; Green, M. A. *J. Am. Chem. Soc.* **2003**, *125*, 5161.
(6) Alexander, M. R.; Thompson, G. E.; Zhou, X.; Beamson, G.; Fairley, N. *Surf. Interface Anal.* **2002**, *34*, 485.
(7) Tanuma, S.; Powell, C. J.; Penn, D. N. *Surf. Interface Anal.* **1994**, *21*, 165.
(8) Vovk, I. E., Emmez, E., Erbudak, M., Bukhtiyarov, V. I., Ozensoy, E. submitted.
(9) Oku, M.; Wagatsuma, K.; Kohiki, S. *Phys. Chem. Chem. Phys.* **1999**, *1*, 5327.
(10) Dissanayake, D.; Kharas, K. C. C.; Lunsford, J. H.; Rosynek, M. P. *J. Catal.* **1993**, *139*, 652.
(11) Desikusumastuti, A.; Happel, M.; Dumbuya, K.; Staudt, T.; Laurin, M.; Gottfried, J. M.; Steinruck, H. P.; Libuda, J. *J. Phys. Chem. C* **2008**, *112*, 6477.
(12) Förster, S.; Widdra, W. *Surf. Sci.* **2010**, *604*, 2163.
(13) Lotnyk, A.; Senz, S.; Hesse, D. *Solid State Ionics* **2006**, *177*, 429.
(14) Warschkow, O.; Wang, Y.; Subramanian, A.; Asta, M.; Marks, L. D. *Phys. Rev. Lett.* **2008**, *100*, 086102.
(15) Wang, Y.; Warschkow, O.; Marks, L. D. *Surf. Sci.* **2007**, *601*, 63.

(16) Sedona, F.; Rizzi, G. A.; Agnoli, S.; Llabres i Xamena, F. X.; Papageorgiou, A.; Ostermann, D.; Sambi, M.; Finetti, P.; Schierbaum, K.; Granozzi, G. *J. Phys. Chem. B* **2005**, *109*, 24411.
(17) Barcaro, G.; Sedona, F.; Fortunelli, A.; Granozzi, G. *J. Phys. Chem. C* **2007**, *111*, 6095.
(18) Erdman, N.; Poeppelmeier, K. R.; Asta, M.; Warschkow, O.; Ellis, D. E.; Marks, L. D. *Nature* **2002**, *419*, 55.
(19) Erdman, N.; Warschkow, O.; Asta, M.; Poeppelmeier, K. R.; Ellis, D. E.; Marks, L. D. *J. Am. Chem. Soc.* **2003**, *125*, 10050.
(20) Russell, B. C.; Castell, M. R. *J. Phys. Chem. C* **2008**, *112*, 6538.
(21) Epling, W. S.; Campbell, L. E.; Yezerets, A.; Currier, N. W.; Parks, J. E. *Catal. Rev.* **2004**, *46*, 163.
(22) Roy, S.; Baiker, A. *Chem. Rev.* **2009**, *109*, 4054.
(23) Ozensoy, E.; Peden, C. H. F.; Szanyi, J. *J. Phys. Chem. B* **2006**, *110*, 17001.
(24) Ozensoy, E.; Peden, C. H. F.; Szanyi, J. *J. Phys. Chem. B* **2006**, *110*, 17009.
(25) Ozensoy, E.; Peden, C. H. F.; Szanyi, J. *J. Catal.* **2006**, *243*, 149.
(26) Andonova, S. M.; Şentürk, G. S.; Kayhan, E.; Ozensoy, E. *J. Phys. Chem. C* **2009**, *113*, 11014.
(27) Andonova, S. M.; Şentürk, G. S.; Ozensoy, E. *J. Phys. Chem. C* **2010**, *114*, 17003.
(28) Hodjati, S.; Vaezzadeh, K.; Petit, C.; Pitchon, V.; Kiennemann, A. *Appl. Catal., B* **2000**, *26*, 5.
(29) Berlich, A.; Strauss, H.; Langheinrich, C.; Chassé, A.; Morgner, H. *Surf. Sci.* **2011**, *605*, 158.
(30) Takahashi, N.; Suda, A.; Hachisuka, I.; Sugiura, M.; Sobukawa, H.; Shinjoh, H. *Appl. Catal., B* **2007**, *72*, 187.
(31) Imagawa, H.; Tanaka, T.; Takahashi, N.; Matsunaga, S.; Suda, A.; Shinjoh, H. *J. Catal.* **2007**, *251*, 315.